



1 **Photoenhanced sulfates formation by the heterogeneous uptake of SO₂ on non-**
2 **photoactive mineral dust**

3 Chong Han*, Jiawei Ma, Wangjin Yang, Hongxing Yang

4 School of Metallurgy, Northeastern University, Shenyang, 110819, China

5 *Address correspondence to author: hanch@smm.neu.edu.cn

6

7 **Short summary.** We provide direct evidences that light prominently enhances the conversion
8 of SO₂ to sulfates on non-photoactive mineral dust, where ³SO₂ can act as a pivotal trigger to
9 generate sulfates. Photochemical sulfate formation depends on H₂O, O₂, and basicity of mineral
10 dust. It is suggested that the SO₂ photochemistry on non-photoactive mineral dust significantly
11 contributes to sulfates, highlighting previously unknown pathway to better explain the missing
12 sources of atmospheric sulfates.

13

14 **Abstract.** Heterogeneous uptake of SO₂ on mineral dust is a predominant formation pathway
15 of sulfates, whereas the contribution of photo-induced SO₂ oxidation to sulfates on the dust
16 interfaces still remains unclear. Here, we investigated heterogeneous photochemical reactions
17 of SO₂ on five mineral oxides (SiO₂, kaolinite, Al₂O₃, MgO, and CaO) without photocatalytic
18 activity. Light significantly enhanced the uptake of SO₂, and its enhancement effects negatively
19 depended on the basicity of mineral oxides. The initial uptake coefficient ($\gamma_{0,BET}$) and the
20 steady-state uptake coefficient ($\gamma_{s,BET}$) of SO₂ positively relied on light intensity, relative
21 humidity (RH) and O₂ content, while they exhibited a negative relationship with the initial SO₂
22 concentration. Rapid sulfate formation during photo-induced heterogeneous reactions of SO₂
23 with all mineral oxides was confirmed to be ubiquitous, and H₂O and O₂ played the key roles
24 in the conversion of SO₂ to sulfates. Specially, ³SO₂ was suggested to be the trigger for
25 photochemical sulfate formation. Atmospheric implications supported a potential contribution
26 of interfacial SO₂ photochemistry on non-photoactive mineral dust to atmospheric sulfate
27 sources.



28

29 **Keywords:** SO₂; Sulfates; Non-photoactive mineral dust; Heterogeneous photochemistry

30

31

32 **1 Introduction**

33 As an important trace gas in the atmosphere, SO₂ is mainly emitted by volcanic eruption and
34 fuel combustion. There is an uneven distribution of atmospheric SO₂ concentrations that show
35 a distinctive seasonal and regional differentiation. Typical ratios of SO₂ in the troposphere are
36 below 0.5 ppb for a clean weather in remote areas, rising to around several hundred ppb during
37 the polluted days in urban regions(Ma et al., 2020). About half of SO₂ is oxidized to sulfates(He
38 et al., 2012), which is one of the most significant compositions in fine particles. Sulfates can
39 contribute greatly to the mass concentration of PM_{2.5}, with the mass of sulfates high up to
40 30%(Shao et al., 2019), especially in polluted regions where high-sulfur fuels are usually
41 used(Olson et al., 2021). They significantly alter physicochemical properties of aerosols in
42 terms of hygroscopicity, acidity and light absorption property(Chan and Chan, 2003; Cao et al.,
43 2013; Lim et al., 2018). Sulfates also pose a human health risk through causing respiratory
44 illness and cardiovascular(Shiraiwa et al., 2017). In addition, the deposition of sulfates leads to
45 adverse effects on ecosystems via the acidification of soils and lakes(Golobokova et al., 2020).
46 Therefore, the oxidation of SO₂ to form sulfates has attracted widespread attentions in the past
47 decades.

48 The conversion of SO₂ to sulfates in the atmosphere usually occur by three ways: gas-phase
49 oxidation of SO₂ by hydroxyl radicals (\bullet OH) or Criegee intermediate radicals(Mauldin et al.,
50 2012; Davis et al., 1979); aqueous-phase reaction of SO₂ with O₃, H₂O₂ or transition metal ions
51 dissolved in cloud and fog droplets(Alexander et al., 2009; Herrmann et al., 2000; Liu et al.,
52 2020a; Li et al., 2020); and heterogeneous SO₂ uptake on aerosols including authentic mineral
53 dust, soot, inorganic ion and organic compounds(Adams et al., 2005; He et al., 2018a; Zhang
54 et al., 2020a; Liu et al., 2020b). However, the oxidation of SO₂ in gas and aqueous phases fails
55 to explain high sulfate concentrations under polluted conditions. Model simulation suggests



56 that the rapid sulfate formation can be attributed to the heterogeneous SO₂ uptake(Li et al.,
57 2017). A positive relationship between the fraction of sulfates and mineral dust in haze days
58 has been reported, implying that mineral dust may account for the formation of sulfates(Wang
59 et al., 2020a). Moreover, a large amount of sulfates was observed to be formed on the surface
60 of mineral dust after long-distance transport(Prospero, 1999). Thus, investigating the
61 heterogeneous oxidation of SO₂ on mineral dust is of fundamental importance to reveal large
62 missing sources of atmospheric sulfates in the haze periods.

63 Mineral dust, regarded as the dominant component of particulate matters in the atmosphere,
64 accounts for about 30%–60% mass fractions of global aerosols(Dentener et al., 1996; Peng et
65 al., 2012). It primarily contains SiO₂ (40%–80%), followed by Al₂O₃ (10%–15%), Fe₂O₃
66 (6%–13%), CaO (3%–10%), MgO (1%–7%) and TiO₂ (0.1%–5%)(Urupina et al., 2021;
67 Urupina et al., 2019; Usher et al., 2003). Mineral dust can provide active sites for adsorption
68 and reaction of gases. Up to now, the heterogeneous SO₂ uptake on authentic mineral aerosols
69 and model mineral oxides has been widely reported(Ma et al., 2019; Goodman et al., 2001;
70 Wang et al., 2018; Wang et al., 2020b), with various uptake coefficients (γ) of SO₂ varying
71 from 10⁻⁹ to 10⁻⁴(Urupina et al., 2019; Usher et al., 2002).

72 It was recognized that light could significantly enhance heterogeneous conversion of SO₂ to
73 sulfates on the surface of photocatalytic mineral dust(Chen et al., 2021; Li et al., 2019; Wang
74 et al., 2020b). Electron-hole pairs are produced via photo-induced electrons from the valence
75 band to the conduction band of photocatalytic metal oxides, and then react with H₂O and O₂ to
76 generate reactive oxygen species (ROS), such as •OH and •O₂⁻(Chu et al., 2019). Sulfates are
77 produced by the heterogeneous reactions of SO₂ and ROS(Park and Jang, 2016; Park et al.,
78 2017; Langhammer et al., 2020; Bounechada et al., 2017). In particular, due to the large
79 abundance of non-photoactive mineral dust (more than 85% mass of total mineral dust in the
80 atmosphere) (Usher et al., 2003; Liu et al., 2022), revealing the photooxidation processes of
81 SO₂ on these mineral dust is of great importance to better reevaluate the sulfate formation on
82 aerosols in the global scale.

83 Hence, photochemical SO₂ uptake and sulfate formation on non-photoactive mineral oxides



84 were firstly investigated using a flow reactor and an *in situ* diffuse reflectance infrared Fourier
85 transform spectroscopy (DRIFTS). The SO₂ conversion to sulfates was examined under various
86 conditions, and the roles of light intensity, SO₂ concentration, H₂O, O₂ and basicity of mineral
87 oxides were determined. Reaction mechanisms and atmospheric implications were proposed,
88 highlighting a new and important pathway accounting for photochemical uptake of SO₂ to form
89 sulfates on the non-photoactive surfaces.

90

91 **2 Experimental methods**

92 **2.1 Materials.**

93 Analytical grade SiO₂ (Sinopharm Chemical Reagent Co., Ltd.), kaolinite (Sinopharm
94 Chemical Reagent Co., Ltd.), Al₂O₃ (Alfa Aesar), MgO (Sigma-Aldrich), and CaO (Sigma-
95 Aldrich) were used in the experiments. Through the nitrogen Brunauer-Emmett-Teller (BET)
96 physisorption analysis, their specific surface areas were detected to be 0.419, 6.407, 8.137,
97 10.948 and 6.944 m² g⁻¹, respectively. The ultraviolet-visible (UV-vis) light absorption spectra
98 of samples in the wavelength range of 300–800 nm were obtained by the Shimadzu UV-2550
99 spectrophotometer, as shown in Figure S1 of the Supporting Information. The solid powder
100 (0.2–5 g) was uniformly dispersed into 10.0 mL ethanol solution. The mixed liquid was poured
101 into a rectangle quartz sample dish (14.0 cm × 7.0 cm) and dried to form a solid coating in an
102 oven at 353 K for 10 h. SO₂ standard gas (50 ppm in N₂, Shenyang Air Liquide Co., LTD) and
103 high purity N₂ and O₂ (99.999 vol.%, Shenyang Air Liquide Co., LTD) were used as received.
104 The solid sample powder (0.2 g) was immersed into 10 ml deionized water (20 mg ml⁻¹), and
105 then the suspension was vigorously stirred for 10 min. The pH of SiO₂, kaolinite, Al₂O₃, MgO
106 and CaO suspension was measured to be 6.27, 6.58, 9.33, 10.61 and 12.72 using a pH meter,
107 respectively, which was employed to characterize the basicity of mineral oxides.

108 **2.2 Rectangular flow reactor.**

109 The uptake experiments of SO₂ on mineral dust were performed in a horizontal rectangular
110 flow reactor (26.0 cm length × 7.5 cm width × 2.0 cm height), which was depicted in Figure
111 S2. The reactor was made of quartz to allow the transmission of light. The temperature was



112 maintained at 298 K by circulating temperature-controlled water through the outer jacket of the
113 reactor. Synthetic air with a N₂/O₂ volume ratio of 4:1 was introduced into the flow reactor,
114 and its total flow rate was 1000 mL min⁻¹. The Reynolds number (*Re*) was calculated to be
115 14.42 (*Re* < 200), indicating a laminar flow state. SO₂ with high purity N₂ (100 mL min⁻¹) as
116 carrier gas were introduced into the reactor through a movable T-shaped injector equipped with
117 six exit holes of 0.2 mm diameter, so that the gas could be uniformly distributed over the width
118 of the reactor. The SO₂ concentration was 40–200 ppb and measured with a SO₂ analyzer
119 (Thermo 43i). Wet N₂ generated with a bubbler containing deionized water was introduced by
120 two parallel inlets on the side of T-shaped injector. Relative humidity (RH, 10%–75%) was
121 controlled by regulating the ratio of dry N₂ to wet N₂ and measured via a hygrometer (Center
122 314). The equivalent layer numbers of water on surface was 0.9–4.0 according to the Brunauer-
123 Emmett-Teller (BET) model (Sumner et al., 2004), and the thickness of the film of adsorbed
124 water varied between 2.7–12 nm at RH=10%–75%. There were three equally spaced exhaust
125 ports to mitigate the outlet turbulence. A xenon lamp (CEL-LAX500, China Education Au-light
126 Co., Ltd) was used to simulate sunlight and vertically located above the reactor. A filter was
127 placed on the reactor to remove the light with wavelengths shorter than 300 nm. The spectrum
128 irradiance of the xenon lamp was displayed in Figure S3 and measured using a calibrated
129 spectroradiometer (ULS2048CL-EVO, Avantes). The spectral irradiance was measured inside
130 the reactor, after passing the water cooling and in the absence of a sample. The total irradiance
131 (0–7.93 × 10¹⁶ photons cm⁻² s⁻¹) on the coating can be adjusted by varying the distance of the
132 xenon lamp to the reactor.

133 **2.3 Uptake coefficient of SO₂.**

134 The heterogeneous reaction kinetics of SO₂ with mineral dust can be described by a pseudo-
135 first-order reaction. SiO₂ was taken as an example, and Figure S4 showed a linear relationship
136 between the natural logarithm of the SO₂ concentration and the reaction time. The apparent rate
137 constant (*k*_{obs, SiO₂}) of SO₂ with SiO₂ can be calculated using the equation 1,

$$138 \frac{\ln(C_0/C_t)}{t} = k_{\text{obs, SiO}_2} \quad (1)$$

139 where *C*₀ and *C*_t (ppb) are the initial SO₂ concentration and the SO₂ concentration at the



140 reaction time t , respectively. The loss of SO_2 on the internal wall of the reactor occurred in
141 blank experiments (Figure S5), which should be deducted for the γ calculation. Assuming that
142 the wall loss was constant in the experiments with and without samples, the geometric uptake
143 coefficient (γ_{geo}) was determined by the equation 2 (Knopf et al., 2007),

$$144 \quad \gamma_{\text{geo}} = \frac{4V(k_{\text{obs, SiO}_2} - k_{\text{obs, wall}})}{S\omega} \quad (2)$$

145 where $k_{\text{obs, SiO}_2}$ and $k_{\text{obs, wall}}$ are the apparent rate constants measured with and without SiO_2
146 samples, respectively; V (m^3), S (m^2) and ω (m s^{-1}) are the volume of the rectangular reactor,
147 the surface area of the sample dish, and the mean molecular speed of SO_2 , respectively.

148 The uptake process of SO_2 on SiO_2 depended on the reaction of SO_2 with SiO_2 and the mass
149 transport of SO_2 to the surface. It can be expressed with the equation 3,

$$150 \quad k'_{\text{r, SiO}_2} = \left[\frac{1}{k_{\text{r, SiO}_2}} - \frac{a}{N_u D} \right]^{-1} \quad (3)$$

151 where $k_{\text{r, SiO}_2} = k_{\text{obs, SiO}_2} - k_{\text{obs, wall}}$; $k'_{\text{r, SiO}_2}$ is the reaction rate constant of SO_2 accounting for the
152 diffusion effect; D ($\text{cm}^2 \text{s}^{-1}$) is the diffusion coefficient of SO_2 in air; a (cm) is one half height
153 of the flow reactor; N_u is the Nusselt numbers obtained with a calculation method from Solbrig
154 and Gidaspow (Solbrig and Gidaspow, 1967), which represents the mass transport. Then, the
155 corrected γ can be calculated by inserting the equation 3 into the equation 2. In our experiments,
156 the correction for γ was estimated to be approximate 10%. Initial uptake coefficients (γ_0) and
157 steady-state uptake coefficients (γ_s) were calculated by averaging the signals within the 1.0 and
158 40–60 min reaction time, respectively.

159 To understand the diffusion depth of SO_2 and determine the interaction of SO_2 with the
160 underlying layers of SiO_2 , the uptake of SO_2 as a function of the SiO_2 mass under irradiation
161 was shown in Figure S6. The γ exhibited a linear increase in the SiO_2 mass range of 0.05–2.0
162 g, while it remained unchanged at the SiO_2 mass > 3.0 g. Therefore, the uptake coefficient of
163 SO_2 in the linear regions was normalized using the BET surface area of SiO_2 by the equation
164 4 (Brunauer et al., 1938),

$$165 \quad \gamma_{\text{BET}} = \frac{S_{\text{geo}} \times \gamma_{\text{geo}}}{S_{\text{BET}} \times m_{\text{SiO}_2}} \quad (4)$$



166 where γ_{BET} is the SO₂ uptake coefficient normalized to the BET surface area; S_{geo} (m²) is the
167 geometric area of the sample dish; S_{BET} (m²) is the BET surface area of SiO₂; m_{SiO_2} (g) is the
168 SiO₂ mass. The same method was also used to calculate the uptake coefficients of SO₂ on other
169 mineral oxides.

170 **2.4 In Situ DRIFTS analysis.**

171 The changes in the chemical compositions on mineral oxides in the SO₂ uptake process were
172 investigated by *in situ* diffuse reflectance Fourier-transform infrared spectroscopy (DRIFTS),
173 which was recorded using the Fourier transform infrared (FTIR) spectrometer (Thermo Nicolet
174 iS50) equipped with a mercury cadmium telluride (MCT) detector. About 14 mg mineral oxides
175 was placed into a stainless-steel cup inside the reaction cell. To remove adsorbed impurities,
176 SiO₂ was purged with a 150 mL min⁻¹ airflow (N₂/O₂ volume ratio = 4:1) at RH=40% for 1 h.
177 Then, a background spectrum of unreacted samples was collected. SO₂ (2 ppm) was introduced
178 into the reaction cell, and the IR spectra was recorded as a function of time at a resolution of 4
179 cm⁻¹ by averaging 100 scans. The light from the xenon lamp (500 W) with a total irradiance of
180 3.22×10^{16} photons cm⁻² s⁻¹ was transmitted into the DRIFTS reaction cell via a fiber.

181

182 **3 Results and discussion**

183 **3.1 Photo-enhanced uptake of SO₂.**

184 Acting as the most abundant mineral oxides, SiO₂ was firstly used to investigate the uptake
185 behaviors of SO₂. As shown in Figure 1A, when SO₂ (80 ppb) was exposed to SiO₂ in the dark,
186 the SO₂ concentration decreased to 70 ppb, and then it quickly increased and reached the steady
187 state after 20 min. Upon exposure to SiO₂ under irradiation, the SO₂ concentration exhibited a
188 greater drop than that in the dark. The deactivation of SO₂ uptake on SiO₂ was very slight after
189 20 mins under irradiation. These suggest that light can significantly promote the heterogeneous
190 reaction of SO₂ on SiO₂. When SO₂ didn't contact with SiO₂, its concentration recovered
191 rapidly. The desorption of SO₂ was observed when SO₂ was isolated from SiO₂ in the dark and
192 under irradiation, indicating that the physical adsorption partially contributed to the SO₂ loss
193 during the photochemical process.



194 The uptake coefficients of SO₂ on SiO₂ as a function of irradiation intensity were shown in
195 Figure 1B. The errors in all figures are the standard deviations of three repetitive experiments.
196 Both $\gamma_{0, \text{BET}}$ and $\gamma_{s, \text{BET}}$ displayed a well linear relationship with the irradiation intensity, further
197 confirming the photochemical nature for the reactions of SO₂ on SiO₂. In particular, $\gamma_{0, \text{BET}}$ and
198 $\gamma_{s, \text{BET}}$ on SiO₂ under simulated solar irradiation was comparable with those (10^{-7} – 10^{-6}) on
199 Gobi Desert dust (GDD) and Arizona Test Dust (ATD) under UV irradiation, which contained
200 photocatalytic metal oxides (Park et al., 2017). As for the SO₂ uptake on TiO₂, $\gamma_{0, \text{BET}}$ and $\gamma_{s, \text{BET}}$
201 were measured to be 10^{-6} and 10^{-7} , respectively, by using the flow tube (Ma et al., 2019), which
202 were similar to our results. Usher et al. (2022) reported a larger γ_{BET} (10^{-4}) on TiO₂ using a
203 Knudsen cell reactor. This difference should be ascribed to the variation in the pressure of
204 Knudsen cell (high vacuum) and flow tube reactor (ambient pressure).

205 Figure 1C shows the evolution of $\gamma_{0, \text{BET}}$ and $\gamma_{s, \text{BET}}$ at different SO₂ concentrations under
206 irradiation. An inverse dependence of $\gamma_{0, \text{BET}}$ and $\gamma_{s, \text{BET}}$ on the SO₂ concentration was observed,
207 meaning that both initial and steady-state uptake reactions were lower efficient at higher SO₂
208 concentrations. The uptake of gases on the solid surfaces usually follows the Langmuir-
209 Hinshelwood (L-H) mechanism (Ammann et al., 2003; Zhang et al., 2020b), suggesting that
210 gaseous molecules are quickly absorbed on the surfaces, and then the reactions occur among
211 the absorbed species. Assuming that the adsorption of SO₂ on SiO₂ is in accord with the
212 Langmuir isotherm, the dependence of γ on the SO₂ concentration can be described by the
213 equation 5 (Zhang et al., 2020b),

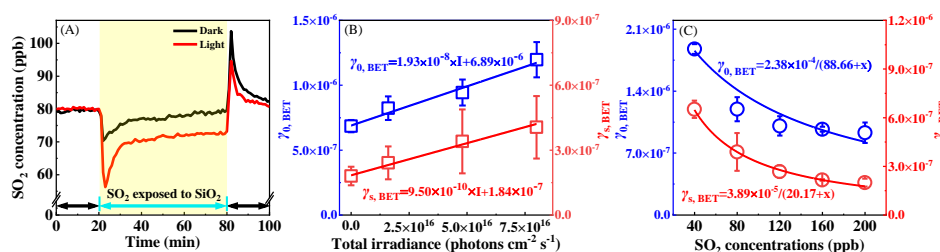
$$214 \quad \gamma = \frac{(4I/S\omega)k[\text{SiO}_2]_{\text{T}}K_{\text{SO}_2}}{1+K_{\text{SO}_2}[\text{SO}_2]_{\text{g}}} \quad (5)$$

215 where $[\text{SO}_2]_{\text{g}}$ is the concentration of gaseous SO₂; $[\text{SiO}_2]_{\text{T}}$ is the total number of active sites
216 on SiO₂; k is the reaction rate constant of SO₂ absorbed on SiO₂; K_{SO_2} represents the Langmuir
217 adsorption constant of SO₂. Because the SiO₂ mass remained constant during the reaction, the
218 equation 5 can be written as the equation 6,



219
$$\gamma = \frac{a}{1 + K_{\text{SO}_2} [\text{SO}_2]_{\text{g}}} \quad (6)$$

220 where $a = (4V/S\omega)k[\text{SiO}_2]K_{\text{SO}_2}$. As shown in Figure 1C, the equation 6 can well describe the
 221 correlation of the SO_2 uptake coefficient with the SO_2 concentration, suggesting that the L-H
 222 mechanism can explain the influence of the SO_2 concentration on $\gamma_{0, \text{BET}}$ and $\gamma_{\text{s, BET}}$.



223
 224 **Figure 1.** (A) The temporal variation of the SO_2 concentration on SiO_2 in the dark and under
 225 irradiation (250 W m^{-2}); The background changes of the SO_2 concentration in the blank
 226 reactor have been deducted. (B) The $\gamma_{0, \text{BET}}$ and $\gamma_{\text{s, BET}}$ of SO_2 on SiO_2 as a function of the
 227 light intensity. (C) The $\gamma_{0, \text{BET}}$ and $\gamma_{\text{s, BET}}$ of SO_2 on SiO_2 at different SO_2 concentrations under
 228 irradiation (250 W m^{-2}); The fitting lines for $\gamma_{0, \text{BET}}$ and $\gamma_{\text{s, BET}}$ were based on the Langmuir-
 229 Hinshelwood mechanism using the equation 6. Reaction conditions: SiO_2 mass of 0.2 g,
 230 temperature of 298 K, RH of 40% and O_2 content of 20%.

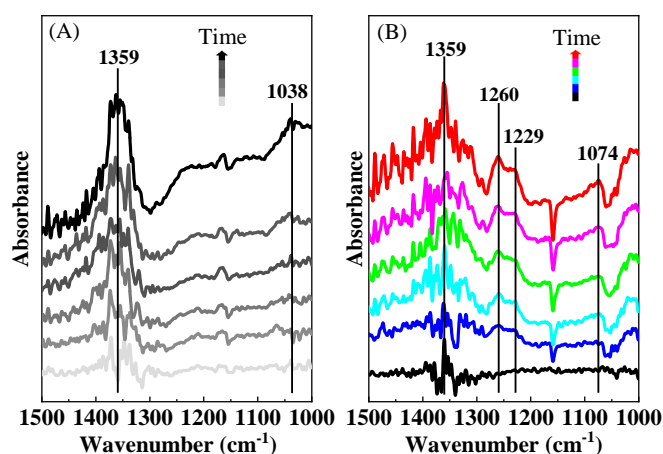
231

232 **3.2 Photo-induced formation of sulfates by the SO_2 uptake.**

233 To investigate the products formed on SiO_2 , *in situ* DRIFTS spectra were recorded, as shown
 234 in Figure 2. The band at 1359 cm^{-1} was assigned to physically-adsorbed SO_2 on SiO_2 (Urupina
 235 et al., 2019). The bidentate sulfate and bisulfate contributed to the bands at 1260 and 1229
 236 cm^{-1} (Urupina et al., 2019; Yang et al., 2020), respectively. The bands at 1074 and 1038 cm^{-1}
 237 may be related to the monodentate sulfite (Yang et al., 2019; Wang et al., 2019). It was noted
 238 that the intensity of physically-adsorbed SO_2 (1359 cm^{-1}) under irradiation was lower than that
 239 in the dark (Figure S7), which may be ascribed to further conversion of SO_2 adsorbed on SiO_2
 240 under irradiation. Especially, the sulfate bands (1260 and 1229 cm^{-1}) appeared under irradiation,



241 while they were not observed in the dark. This clearly confirms the crucial role of light in the
 242 heterogeneous conversion of SO₂ to sulfates on SiO₂. The bands of sulfites (1038 and 974 cm⁻¹)
 243 under dark and irradiation conditions became more apparent with the reaction time, suggesting
 244 the continuous formation of sulfites.



245

246 **Figure 2.** *In situ* DRIFTS spectra of SiO₂ during the uptake process of SO₂ (2 ppm) in the
 247 dark (A) and under irradiation (B). Reaction conditions: RH of 40%, temperature of 298 K
 248 and O₂ content of 20%.

249

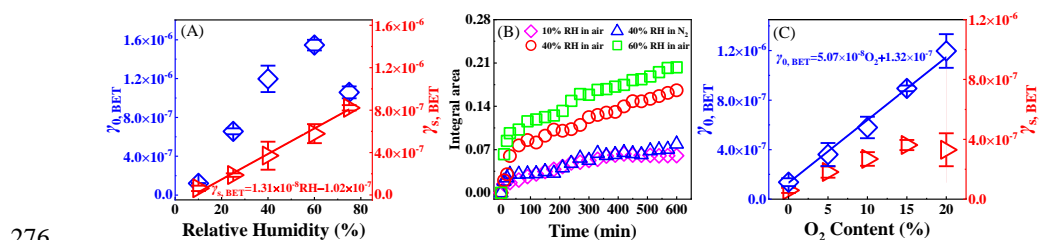
250 3.3 Key roles of H₂O and O₂ in photochemical conversion of SO₂ to sulfates.

251 Figure S8A shows temporal variations of the SO₂ concentration in the reaction with SiO₂ at
 252 RH=10% and 60% under irradiation. The uptake of SO₂ was very weak at RH=10%, whereas
 253 it was obvious at RH=60%. Moreover, H₂O markedly prolonged the time to reach the steady-
 254 state uptake of SO₂. This definitely determines that H₂O plays a distinct enhancement role in
 255 the photochemical uptake of SO₂. As shown in Figure 3A, $\gamma_{0, \text{BET}}$ had a continuous increase
 256 from $(1.20 \pm 0.04) \times 10^{-7}$ to $(1.54 \pm 0.07) \times 10^{-6}$ with increasing the RH in the 10%–60% range,
 257 but it decreased to $(1.05 \pm 0.09) \times 10^{-6}$ at RH=75%. The $\gamma_{s, \text{BET}}$ linearly depended on the RH,
 258 and linear fitting to $\gamma_{s, \text{BET}}$ versus RH yielded the equation $\gamma_{s, \text{BET}} = 1.31 \times 10^{-8} \times \text{RH} - 1.02 \times 10^{-7}$.
 259 Adsorbed H₂O promoted the hydration and dissociation of SO₂ (Huang et al., 2015), and it may



260 generate reactive oxygen species (ROS) such as $\bullet\text{OH}$ or HO_2 radicals to oxidize SO_2 under
 261 irradiation (Li et al., 2020; Ma et al., 2019), which would lead to positive effects of RH on the
 262 SO_2 uptake. Adsorbed H_2O also occupied adsorptive and active sites on the surface, and
 263 produced the competition with SO_2 . When this competitive role was dominated, the uptake of
 264 SO_2 would be hindered.

265 The DRIFTS spectra of SiO_2 during the SO_2 uptake at different RHs are shown in Figure
 266 S9A. The band intensities of sulfates (1260 and 1229 cm^{-1}) at $\text{RH}=60\%$ were greatly stronger
 267 than those at $\text{RH}=10\%$, suggesting that H_2O significantly promotes the sulfate formation. To
 268 further investigate the influence of H_2O on the sulfate formation, the integrated area of sulfates
 269 in the DRIFTS spectra ($1289\text{--}1202\text{ cm}^{-1}$) as a function of the time at different RHs is illustrated
 270 in Figure 3B. Sulfates exhibited a fast formation in the initial 30 min at any RH, and then they
 271 were continuously generated at a relatively slow rate. Adsorptive sites for SO_2 can be blocked
 272 because of the accumulation of H_2O and products (sulfites and sulfates), resulting in the gradual
 273 deactivation of the surface. It was noted that sulfates had a more distinct formation trend with
 274 increasing the RH, revealing that H_2O can act as an important participator in the production of
 275 sulfates by the photochemical uptake of SO_2 on SiO_2 .



276 **Figure 3.** (A) The dependence of $\gamma_{0, \text{BET}}$ and $\gamma_{s, \text{BET}}$ on RH. (B) Integrated area of sulfates in
 277 *in situ* DRIFTS spectra ($1289\text{--}1202\text{ cm}^{-1}$) as a function of time. (C) The dependence of
 278 $\gamma_{0, \text{BET}}$ and $\gamma_{s, \text{BET}}$ on O_2 . Reaction conditions: SiO_2 mass of 0.2 g , irradiation intensity of 250
 279 W m^{-2} , temperature of 298 K , O_2 content of 20% for (A) and RH of 40% for (B).

280
 281
 282 Figure S8B displays effects of O_2 on the photochemical uptake of SO_2 on SiO_2 . Negligible
 283 SO_2 uptake occurred in N_2 , while there was a significant decrease in the SO_2 concentration in



284 air. The $\gamma_{0, \text{BET}}$ greatly increased from $(1.37 \pm 0.45) \times 10^{-7}$ in N_2 to $(1.19 \pm 0.13) \times 10^{-6}$ in 20%
285 O_2 (Figure 3C), confirming that O_2 was involved in the photochemical reaction of SO_2 on SiO_2 .
286 The $\gamma_{s, \text{BET}}$ displayed different dependence behaviors on O_2 . It exhibited an increase from $(7.10$
287 $\pm 2.85) \times 10^{-8}$ in N_2 to $(4.37 \pm 0.58) \times 10^{-7}$ in 15% O_2 , whereas it remained unchanged in 20%
288 O_2 .

289 DRIFTS spectra of SiO_2 during the SO_2 uptake in N_2 and air was compared in Figure S9B.
290 In both air and N_2 , the bands of absorbed SO_2 (1359 cm^{-1}), sulfates (1260 and 1229 cm^{-1}) and
291 sulfites (1074 cm^{-1}) appeared. Nevertheless, their intensities in N_2 were weaker than those in
292 air. According to the integrated area of sulfates in the DRIFTS spectra ($1289\text{--}1202 \text{ cm}^{-1}$) as a
293 function of time, the formation trends of sulfates were similar in N_2 and air (Figure 3B), while
294 the sulfate formation rate in N_2 was obviously lower than that in air, meaning that O_2 enhanced
295 the sulfate production. It was reported that the production rate of sulfates from the SO_2 uptake
296 on TiO_2 and by the photolysis of nitrates under UV irradiation in N_2 was also smaller than that
297 in air (Ma et al., 2019; Gen et al., 2019b). In addition, it was noted that sulfates can be generated
298 in N_2 , meaning that O_2 was not necessary and some pathways contributed to sulfates without
299 O_2 .

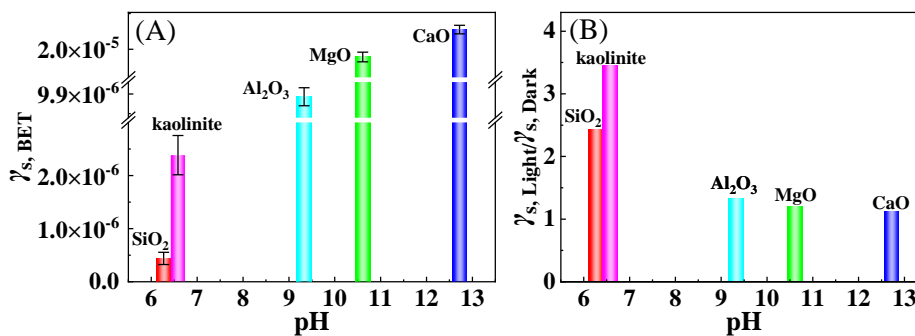
300

301 **3.4 Ubiquitously photoenhanced conversion of SO_2 to sulfates.**

302 To better assess the potential for photochemical conversion of SO_2 to sulfates, the SO_2 uptake
303 experiments were further performed for typical mineral oxides without photocatalytic activity.
304 As displayed in Figure S10, more obvious uptake behaviors of SO_2 on kaolinite, Al_2O_3 , MgO
305 and CaO were observed under irradiation when compared to those in the dark. Figure 4A shows
306 that there was the largest $\gamma_{s, \text{BET}}$ for CaO among five minerals, and $\gamma_{s, \text{BET}}$ positively depended
307 on the basicity (pH) of mineral oxides. Basic oxides generally contains more surface hydroxyls,
308 which is in favor of sulfite and sulfate formation to enhance the heterogeneous uptake of
309 SO_2 (Zhang et al., 2006). Moreover, the ratios of steady-state uptake coefficients under
310 irradiation to those in the dark ($\gamma_{s, \text{Light}}/\gamma_{s, \text{Dark}}$) were larger than 1.0 for all mineral oxides



311 (Figure 4B), determining a general enhancement role of light in the SO_2 uptake. However, the
 312 $\gamma_{\text{Light}}/\gamma_{\text{Dark}}$ had smaller values with an increase in the basicity, suggesting that the promotion
 313 effect of the light was less remarkable for basic oxides.



314

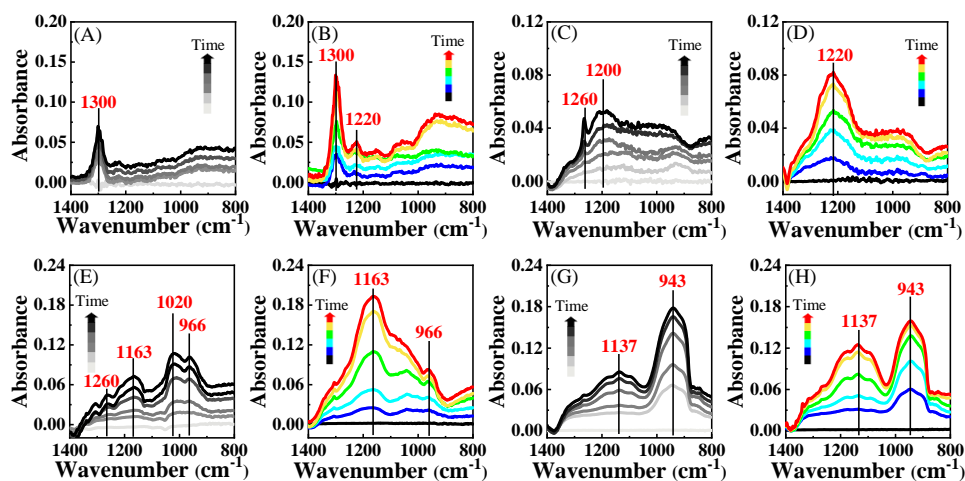
315 **Figure 4.** (A) The dependence of $\gamma_{s, \text{BET}}$ under irradiation on the basicity (pH) of mineral
 316 oxides. (B) The ratios of steady-state uptake coefficients under irradiation to those in the dark
 317 ($\gamma_{s, \text{Light}}/\gamma_{s, \text{Dark}}$) for different mineral oxides. Reaction conditions: mineral oxides mass of 0.2
 318 g, irradiation intensity of 250 W m^{-2} , temperature of 298 K, RH of 40% and O_2 content of
 319 20%.

320

321 As shown in Figure 5A and B, no formation of sulfates was found for kaolinite in the dark,
 322 while bisulfates (1220 cm^{-1}) were observed under irradiation. Compared to weaker peaks of
 323 sulfates (1200 and 1260 cm^{-1}) for Al_2O_3 in the dark (Figure 5C), a stronger band of bisulfates
 324 appeared at 1220 cm^{-1} under irradiation (Figure 5D). By contrast to the generation of sulfates
 325 for kaolinite and Al_2O_3 , both sulfites and sulfates formations were observed for MgO and CaO
 326 (Figure 5E-H). Sulfites were dominant in the dark, as shown by the peaks at 966 and 1020 cm^{-1}
 327 for MgO and 943 cm^{-1} for CaO, whereas the sulfate formation was significantly enhanced
 328 under irradiation according to peak intensities at 1163 cm^{-1} for MgO and 1137 cm^{-1} for CaO.
 329 It should be noted that these mineral oxides were non-photoactive because of their poor light
 330 absorption property (Figure S1). Nevertheless, it was very surprised that the light can greatly
 331 promote the formation of sulfates via the SO_2 uptake process on mineral oxides without



332 photocatalytic activity, which was strongly suggested to be a new and important finding for
 333 atmospheric sulfate sources.



334
 335 **Figure 5.** *In situ* DRIFTS spectra of kaolinite (A and B), Al₂O₃ (C and D), MgO (E and F),
 336 CaO (G and H) during the uptake process of SO₂ (2 ppm) for 600 min in the dark (black
 337 lines) and under irradiation (colorful lines). Reaction conditions: RH of 40%, temperature of
 338 298 K and O₂ content of 20%.

339

340 3.5 Conversion mechanisms of SO₂ to sulfates.

341 Heterogeneous photochemical reaction mechanisms of SO₂ on non-photoactive mineral dust
 342 were proposed in light of experimental observations (Figure 6). Gaseous SO₂ was adsorbed on
 343 the surface (R1), and then reacted with H₂O to form sulfites (R2). Under irradiation, adsorbed
 344 SO₂ accepted photons to form its singlet states (¹SO₂) and triplet states (³SO₂) (R3–5)
 345 (Sidebottom et al., 1972; Martins-Costa et al., 2018). The reaction between ³SO₂ and H₂O
 346 resulted in the formation of HOSO• and •OH (R6), which can combine with SO₂ to produce
 347 HOSO₂• (R7). HOSO• and HOSO₂• can be transformed into SO₃, which reacted with H₂O to
 348 drove the sulfate formation (R8 and R9). The interaction between ³SO₂ and O₂ may also
 349 generate SO₃ directly, which would be converted to sulfates subsequently (R10). Theoretical
 350 calculations suggested that the multistep reactions between ³SO₂ with H₂O and O₂ had small
 351 energy barriers or were barrier-free (Gong et al., 2022), which could enhance the generation of

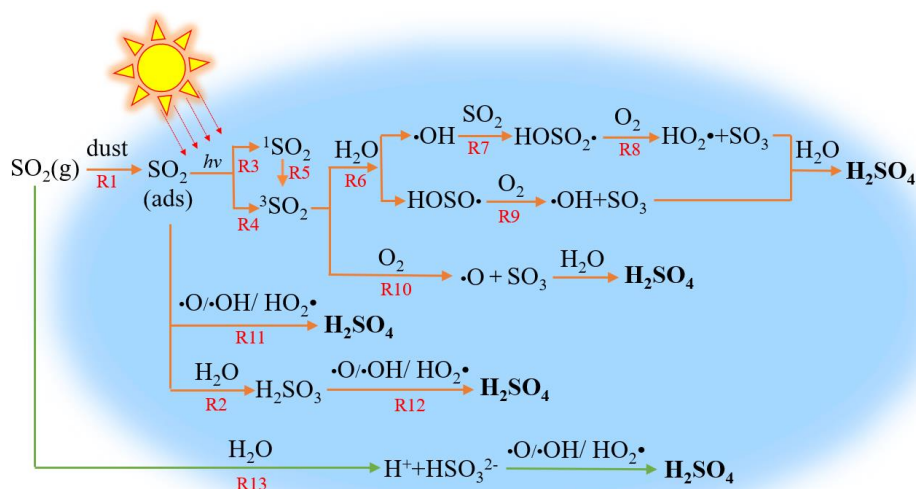


352 ROS and the transformation of S(IV) to S(VI). As displayed by R11 and R12, SO₂ and H₂SO₃
353 adsorbed on the surface may be oxidized to form sulfates via the reactions with ROS including
354 •O, •OH or HO₂•, which were produced in R6 and R8-10. In addition, gaseous SO₂ could be
355 dissolved into adsorbed H₂O to generate bisulfites, which would be finally converted to sulfates
356 by ROS (R13) (Urupina et al., 2019). As displayed in Figure S11A, the IR peaks of sulfates
357 were not observed when tris (2,2'-bipyridine) ruthenium dihydrochloride (Ru(bpy)₃(Cl)₂) was
358 employed as the quencher of ³SO₂ (Bulgakov and Safonova, 1996). The peaks were assigned to
359 the vibrations of excited Ru(bpy)₃(Cl)₂ (Mukuta et al., 2014). This definitely proves that ³SO₂
360 is the key trigger for the sulfate formation. NaHCO₃ can be used as an efficient •OH scavenger
361 to determine the role of •OH deriving from the ³SO₂ reactions (Gen et al., 2019a). Figure S11B
362 shows that the peaks of sulfates were obviously weaker in the presence of NaHCO₃, confirming
363 the dominant contribution of •OH formed in R6 and R9 to the formation of sulfates.

364 Several photochemical mechanisms have been reported to explain the sulfate formation via
365 the SO₂ uptake on various surfaces. Photoactive mineral oxides (such as TiO₂, F₂O₃ and ZnO)
366 can accept photons to produce electron-hole pairs, which generated ROS for the conversion of
367 SO₂ to sulfates (Ma et al., 2019; Li et al., 2019; Wang et al., 2020b). For example, •OH and
368 HO₂•, generated from the reaction of hole with H₂O and electron with O₂, respectively, can act
369 as oxidizing agents for the reaction with SO₂ (Ma et al., 2019). Similarly, the reaction of SO₂
370 with photo-induced •OH obviously enhanced the formation of sulfate on diesel soot and actual
371 PM_{2.5} (Zhang et al., 2022; Zhang et al., 2020c). NO₂ and NO₂⁻/HNO₂ can be formed in the
372 nitrates photolysis, and primarily contributed to the oxidation of SO₂ to sulfates on nitrates (Gen
373 et al., 2019b; Gen et al., 2019a). Theoretically, the mechanism proposed in this study should
374 also occur on photo-excited substrates. Taking TiO₂ as an example, SO₂ competed with TiO₂
375 for photons, and the production efficiency of ³SO₂ and excited state of TiO₂ (TiO₂^{*}) depended
376 on their light absorption properties. Meanwhile, ³SO₂ had a competition electron-hole pairs
377 generated from TiO₂^{*} for O₂ and H₂O. Thus, the dominant mechanism for the SO₂ uptake on
378 TiO₂ should be related to light absorption properties of precursors and the reactivity for ³SO₂
379 and TiO₂^{*} to O₂ and H₂O. By contrast, all mineral oxides used here cannot be excited under



380 irradiation according to their light absorption spectra (Figure S1). Nevertheless, SO₂ adsorbed
 381 on mineral oxides can absorb the ultraviolet radiation (290–400 nm) to form the excited states
 382 of SO₂ (SO₂^{*})(Kroll et al., 2018), which subsequently reacted with H₂O and O₂, finally
 383 converting SO₂ to sulfates. It means that any surfaces, providing absorptive sites for SO₂, can
 384 significantly enhance the photooxidation of SO₂ to sulfates.



385

386 **Figure 6.** The proposed photochemical conversion mechanisms of SO₂ to sulfates on non-
 387 photoactive mineral dust.

388

389 4 Atmospheric implications

390 The lifetime (τ) for photochemical loss of SO₂ on mineral dust was given using the equation
 391 7,

$$392 \quad \tau = \frac{4}{\gamma \omega A} \quad (7)$$

393 where γ and ω are the uptake coefficient and the mean molecular speed of SO₂, respectively; A
 394 is the surface area density of mineral dust, and it is estimated to be $(1.4\text{--}4.8) \times 10^{-5} \text{ cm}^2$
 395 cm^{-3} (Zhang et al., 2019; He et al., 2018b). In this work, $\gamma_{s, \text{BET}}$ of SO₂ on several mineral oxides
 396 were measured to be from 4.39×10^{-7} to 3.45×10^{-5} under conditions with SO₂ concentration
 397 of 40 ppb, irradiation intensity of 250 W m^{-2} and RH of 40%. Thus, the τ of SO₂ with respect



398 to the photooxidation on mineral dust was calculated to be 0.9–240 days, which was shorter
399 than that (54 years) for the photochemical uptake of SO₂ on TiO₂ and the corresponding one
400 (346 days) for the heterogeneous oxidation of SO₂ on ATD in the presence of nitrates(Ma et al.,
401 2019; Zhang et al., 2019). It should be pointed out that the content of TiO₂ in mineral dust was
402 only about 1%, and thus the surface area density of TiO₂ was about 10⁻⁷ cm² cm⁻³, leading to
403 a longer τ (54 years) for the loss of SO₂ on TiO₂(Ma et al., 2019). It was comparable to the
404 lifetime (3.6–20 days) of SO₂ for the gas-phase reaction with •OH at a concentration of ~10⁻⁶
405 molecules cm⁻³(Huang et al., 2015; Zhang et al., 2019). Therefore, the photochemical process
406 with the excited state SO₂ acting as a driver on mineral dust was an important pathway for the
407 SO₂ sink in the atmosphere.

408 Sulfates show significant influences on the atmosphere, such as an important contributor to
409 the haze formation, affecting the activity of aerosols acting as cloud condensation nuclei (CCN)
410 and ice nuclei (IN), and modifying optical property and acidity of aerosols. A sulfate formation
411 rate (R) can be obtained using γ by the equation 8(Cheng et al., 2016),

$$412 \quad R = \frac{d[SO_4^{2-}]}{dt} = \left[\frac{R_p}{D} + \frac{4}{\gamma\omega} \right]^{-1} A[SO_2] \quad (8)$$

413 where R_p is the radius of mineral dust, which can be estimated using the equation 9(Li et al.,
414 2020),

$$415 \quad R_p = (0.254 \times [PM_{2.5}]/(\mu\text{g m}^{-3}) + 10.259) \times 10^{-9} \text{ m} \quad (9)$$

416 where $[PM_{2.5}]$ was average PM_{2.5} mass concentration, and 300 $\mu\text{g m}^{-3}$ was used for the polluted
417 periods in typical China cities(Li et al., 2020; Guo et al., 2014). It was assumed that mineral
418 dust accounted for 50% mass of PM_{2.5}(Tohidi et al., 2022), and the mass fraction of SiO₂, Al₂O₃,
419 MgO, and CaO in mineral dust was 60%, 12.5%, 4% and 6.5%, respectively(Urupina et al.,
420 2021; Urupina et al., 2019; Usher et al., 2003). Thus, R was determined to be 2.15 $\mu\text{g m}^{-3} \text{ h}^{-1}$
421 according to $\gamma_{s, \text{BET}}$ under environmental conditions above. Table S1 summarizes sulfate
422 formation rates from various SO₂ oxidation pathways, including gas-phase reaction with
423 •OH(Xue et al., 2016), aqueous-phase oxidation by dissolved NO₂, H₂O₂ and TMI
424 catalysis(Cheng et al., 2016; Liu et al., 2020a; Ye et al., 2021), and heterogeneous



425 photochemistry on the surfaces of nitrates (Gen et al., 2019a), brown carbon (Liu et al., 2020b),
426 black carbon and PM_{2.5} (Zhang et al., 2022; Zhang et al., 2020c). It was clearly noted that sulfate
427 formation rates on non-photocatalytic mineral oxides under simulated sunlight were
428 comparable with those (0.001–10 μg m⁻³ h⁻¹) for various pathways above, which may explain
429 the missing sulfate sources in the atmosphere. Accordingly, this new sulfate pathway should be
430 well taken into the full consideration in further field observation and model simulation studies
431 to better quantify atmospheric sulfate formation.

432

433 **Author contributions**

434 CH and JM designed and conducted experiments; CH and JM analyzed the data and prepared
435 the paper with contributions from WY and HY. CH supervised the project.

436

437 **Competing interests**

438 The authors declare that they have no conflict of interest.

439

440 **Acknowledgements**

441 This work was supported by the National Natural Science Foundation of China [grant number
442 42077198], the LiaoNing Revitalization Talents Program [grant number XLYC1907185], and
443 the Fundamental Research Funds for the Central Universities [grant numbers N2025011].

444

445 **Reference**

- 446 Adams, J., Rodriguez, D., and Cox, R.: The uptake of SO₂ on Saharan dust: A flow tube study,
447 *Atmos. Chem. Phys.*, 5, 2679–2689, <https://doi.org/10.5194/acpd-5-2643-2005>, 2005.
- 448 Alexander, B., Park, R. J., Jacob, D. J., and Gong, S.: Transition metal-catalyzed oxidation of
449 atmospheric sulfur: Global implications for the sulfur budget, *J. Geophys. Res.*, 114, 2309–
450 2312, <https://doi.org/10.1029/2008jd010486>, 2009.
- 451 Ammann, M., Poschl, U., and Rudich, Y.: Effects of reversible adsorption and Langmuir–
452 Hinshelwood surface reactions on gas uptake by atmospheric particles, *Phys. Chem. Chem.*
453 *Phys.*, 5, 351–356, <https://doi.org/10.1039/b208708a>, 2003.
- 454 Bounechada, D., Anderson, D., Skoglundh, M., and Carlsson, P.: SO₂ adsorption on silica
455 supported iridium, *J. Chem. Phys.*, 146, 084701–084708, <https://doi.org/10.1063/1.4976835>,



- 456 2017.
- 457 Brunauer, B., Deming, L., Deming, W., and Teller, E.: Adsorption of gases in multimolecular
458 layers, *J. Am. Chem. Soc.*, 60, 309-319, <https://doi.org/10.1021/ja01269a023>, 1938.
- 459 Bulgakov, R. G. and Safonova, L. A.: Chemiluminescence in the oxidation of Na₂S by oxygen
460 in water solutions, *Russ. Chem. Bull.*, 45, 1775-1776, <https://doi.org/10.1007/bf01431827>,
461 1996.
- 462 Cao, J., Tie, X., Dabberdt, W. F., Jie, T., Zhao, Z., An, Z., Shen, Z., and Feng, Y.: On the
463 potential high acid deposition in northeastern China, *J. Geophys. Res.: Atmos.*, 118, 4834-
464 4846, <https://doi.org/10.1002/jgrd.50381>, 2013.
- 465 Chan, M. and Chan, C.: Hygroscopic properties of two model humic-like substances and their
466 mixtures with inorganics of atmospheric importance, *Environ. Sci. Technol.*, 37, 5109-5115,
467 <https://doi.org/10.1021/es034272o>, 2003.
- 468 Chen, Y., Tong, S., Li, W., Liu, Y., Tan, F., Ge, M., Xie, X., and Sun, J.: Photocatalytic oxidation
469 of SO₂ by TiO₂: Aerosol formation and the key role of gaseous reactive oxygen species,
470 *Environ. Sci. Technol.*, 55, 9784-9793, <https://doi.org/10.1021/acs.est.1c01608>, 2021.
- 471 Cheng, Y., Zheng, G., Wei, C., Mu, Q., Zheng, B., Wang, Z., Gao, M., Zhang, Q., He, K.,
472 Carmichael, G., Pöschl, U., and Su, H.: Reactive nitrogen chemistry in aerosol water as a
473 source of sulfate during haze events in China, *Sci. Adv.*, 2, 1601530-1601540,
474 <https://doi.org/10.1126/sciadv.1601530>, 2016.
- 475 Chu, B., Wang, Y. L., Yang, W. W., Ma, J. Z., Ma, Q. X., Zhang, P., Liu, Y. C., and He, H.:
476 Effects of NO₂ and C₃H₆ on the heterogeneous oxidation of SO₂ on TiO₂ in the presence or
477 absence of UV-Vis irradiation, *Atmos. Chem. Phys.*, 19, 14777-14790,
478 <https://doi.org/10.5194/acp-19-14777-2019>, 2019.
- 479 Davis, D. D., Ravishankara, A. R., and Fischer, S.: SO₂ oxidation via the hydroxyl radical:
480 Atmospheric fate of HSO_x radicals, *Geo. Res. Lett.*, 6, 113-116,
481 <https://doi.org/10.1029/GL006i002p00113>, 1979.
- 482 Dentener, F., Carmichael, G., Zhang, Y., Lelieveld, J., and Crutzen, P.: Role of mineral aerosol
483 as a reactive surface in the global troposphere, *J. Geophys. Res.: Atmos.*, 101, 22869-22889,
484 <https://doi.org/10.1029/96jd01818>, 1996.
- 485 Gen, M., Zhang, R., Huang, D., Li, Y., and Chan, C.: Heterogeneous oxidation of SO₂ in sulfate
486 production during nitrate photolysis at 300 nm: Effect of pH, relative humidity, irradiation
487 intensity, and the presence of organic compounds, *Environ. Sci. Technol.*, 53, 8757-8766,
488 <https://doi.org/10.1021/acs.est.9b01623>, 2019a.
- 489 Gen, M., Zhang, R., Huang, D., Li, Y., and Chan, C.: Heterogeneous SO₂ oxidation in sulfate
490 formation by photolysis of particulate nitrate, *Environ. Sci. Tech. Lett.*, 6, 86-91,
491 <https://doi.org/10.1021/acs.estlett.8b00681>, 2019b.
- 492 Golobokova, L., Khodzher, T., Khuriganova, O., Marinayte, I., Onishchuk, N., Rusanova, P.,
493 and Potemkin, V.: Variability of chemical properties of the atmospheric aerosol above lake
494 baikal during large wildfires in siberia, *Atmosphere*, 11, 1230-1250,
495 <https://doi.org/10.3390/atmos11111230>, 2020.
- 496 Gong, C., Yuan, X., Xing, D., Zhang, D., Martins-Costa, M. T. C., Anglada, J. M., Ruiz-Lopez,
497 M. F., Francisco, J. S., and Zhang, X.: Fast sulfate formation initiated by the spin-forbidden



- 498 excitation of SO₂ at the air-water interface, *J. Am. Chem. Soc.*, 144, 22302-22308,
499 <https://doi.org/10.1021/jacs.2c10830>, 2022.
- 500 Goodman, A., Li, P., Usher, C., and Grassian, V.: Heterogeneous uptake of sulfur dioxide on
501 aluminum and magnesium oxide particles, *J. Phys. Chem. A* 105, 6109-6120,
502 <https://doi.org/10.1021/jp004423z>, 2001.
- 503 Guo, S., Hu, M., Zamora, M. L., Peng, J., Shang, D., Zheng, J., Du, Z., Wu, Z., Shao, M., Zeng,
504 L., Molina, M. J., and Zhang, R.: Elucidating severe urban haze formation in China, *Proc.*
505 *Natl. Acad. Sci. U. S. A.*, 111, 17373-17378, <https://doi.org/10.1073/pnas.1419604111>,
506 2014.
- 507 He, G., Ma, J., and He, H.: Role of carbonaceous aerosols in catalyzing sulfate formation, *ACS*
508 *Catal.*, 8, 3825-3832, <https://doi.org/10.1021/acscatal.7b04195>, 2018a.
- 509 He, H., Li, C., Loughner, C. P., Li, Z., Krotkov, N. A., Yang, K., Wang, L., Zheng, Y., Bao, X.,
510 Zhao, G., and Dickerson, R. R.: SO₂ over central China: Measurements, numerical
511 simulations and the tropospheric sulfur budget, *J. Geophys. Res.: Atmos.*, 117, 37-51,
512 <https://doi.org/10.1029/2011jd016473>, 2012.
- 513 He, P., Alexander, B., Geng, L., Chi, X., Fan, S., Zhan, H., Kang, H., Zheng, G., Cheng, Y., Su,
514 H., Liu, C., and Xie, Z.: Isotopic constraints on heterogeneous sulfate production in Beijing
515 haze, *Atmos. Chem. Phys.*, 18, 5515-5528, <https://doi.org/10.5194/acp-18-5515-2018>,
516 2018b.
- 517 Herrmann, H., Ervens, B., Jacobi, H. W., Wolke, R., Nowacki, P., and Zellner, R.: CAPRAM_{2.3}:
518 A chemical aqueous phase radical mechanism for tropospheric chemistry, *J. Atmos. Chem.*,
519 36, 231-284, <https://doi.org/10.1023/A:1006318622743>, 2000.
- 520 Huang, L., Zhao, Y., Li, H., and Chen, Z.: Kinetics of heterogeneous reaction of sulfur dioxide
521 on authentic mineral dust: Effects of relative humidity and hydrogen peroxide, *Environ. Sci.*
522 *Technol.*, 49, 10797-10805, <https://doi.org/10.1021/acs.est.5b03930>, 2015.
- 523 Knopf, D., Cosman, L., Mousavi, P., Mokamati, S., and Bertram, A.: A novel flow reactor for
524 studying reactions on liquid surfaces coated by organic monolayers: Methods, validation,
525 and initial results, *J. Phys. Chem. A*, 111, 11021-11032, <https://doi.org/10.1021/jp075724c>,
526 2007.
- 527 Kroll, J., Frandsen, B., Kjaergaard, H., and Vaida, V.: Atmospheric hydroxyl radical source:
528 Reaction of triplet SO₂ and water, *J. Phys. Chem. A*, 122, 4465-4469,
529 <https://doi.org/10.1021/acs.jpca.8b03524>, 2018.
- 530 Langhammer, D., Kullgren, J., and Osterlund, L.: Photoinduced adsorption and oxidation of
531 SO₂ on anatase TiO₂, *J. Am. Chem. Soc.*, 142, 21767-21774,
532 <https://doi.org/10.1021/jacs.0c09683>, 2020.
- 533 Li, G., Bei, N., Cao, J., Huang, R., Wu, J., Feng, T., Wang, Y., Liu, S., Zhang, Q., Tie, X., and
534 Molina, L. T.: A possible pathway for rapid growth of sulfate during haze days in China,
535 *Atmos. Chem. Phys.*, 17, 3301-3316, <https://doi.org/10.5194/acp-17-3301-2017>, 2017.
- 536 Li, J., Zhang, Y. L., Cao, F., Zhang, W., Fan, M., Lee, X., and Michalski, G.: Stable sulfur
537 isotopes revealed a major role of transition-metal ion-catalyzed SO₂ oxidation in haze
538 episodes, *Environ. Sci. Technol.*, 54, 2626-2634, <https://doi.org/10.1021/acs.est.9b07150>,
539 2020.



- 540 Li, K., Kong, L., Zhanzakova, A., Tong, S., Shen, J., Wang, T., Chen, L., Li, Q., Fu, H., and
541 Zhang, L.: Heterogeneous conversion of SO₂ on nano α-Fe₂O₃: the effects of morphology,
542 light illumination and relative humidity, *Environ. Sci.: Nano*, 6, 1838-1851,
543 <https://doi.org/10.1039/c9en00097f>, 2019.
- 544 Lim, S., Lee, M., Kim, S., and Laj, P.: Sulfate alters aerosol absorption properties in East Asian
545 outflow, *Sci. Rep.*, 8, 5172-5178, <https://doi.org/10.1038/s41598-018-23021-1>, 2018.
- 546 Liu, T., Clegg, S., and Abbatt, J.: Fast oxidation of sulfur dioxide by hydrogen peroxide in
547 deliquesced aerosol particles, *Proc. Natl. Acad. Sci. U. S. A.*, 117, 1354-1359,
548 <https://doi.org/10.1073/pnas.1916401117>, 2020a.
- 549 Liu, Y., Wang, T., Fang, X., Deng, Y., Cheng, H., Bacha, A. U., Nabi, I., and Zhang, L.: Brown
550 carbon: An underlying driving force for rapid atmospheric sulfate formation and haze event,
551 *Sci. Total. Environ.*, 734, 139415-139424, <https://doi.org/10.1016/j.scitotenv.2020.139415>,
552 2020b.
- 553 Liu, Y., Deng, Y., Liu, J., Fang, X., Wang, T., Li, K., Gong, K., Bacha, A. U., Nabi, I., Ge, Q.,
554 Zhang, X., George, C., and Zhang, L.: A novel pathway of atmospheric sulfate formation
555 through carbonate radicals, *Atmos. Chem. Phys.*, 22, 9175-9197,
556 <https://doi.org/10.5194/acp-22-9175-2022>, 2022.
- 557 Ma, J., Dörner, S., Donner, S., Jin, J. L., Cheng, S. Y., Guo, J. R., Zhang, Z. F., Wang, J. Q.,
558 Liu, P., Zhang, G. Q., Pukite, J., Lampel, J., and Wagner, T.: MAX-DOAS measurements of
559 NO₂, SO₂, HCHO, and BrO at the Mt. Waliguan WMO GAW global baseline station in the
560 Tibetan Plateau, *Atmos. Chem. Phys.*, 20, 6973-6990, [https://doi.org/10.5194/acp-20-6973-](https://doi.org/10.5194/acp-20-6973-2020)
561 [2020](https://doi.org/10.5194/acp-20-6973-2020), 2020.
- 562 Ma, Q., Wang, L., Chu, B., Ma, J., and He, H.: Contrary role of H₂O and O₂ in the kinetics of
563 heterogeneous photochemical reactions of SO₂ on TiO₂, *J. Phys. Chem. A.*, 123, 1311-1318,
564 <https://doi.org/10.1021/acs.jpca.8b11433>, 2019.
- 565 Martins-Costa, M., Anglada, J., Francisco, J., and Ruiz-Lopez, M.: Photochemistry of SO₂ at
566 the air-water interface: A source of OH and HOSO radicals, *J. Am. Chem. Soc.*, 140, 12341-
567 12344, <https://doi.org/10.1021/jacs.8b07845>, 2018.
- 568 Mauldin, R., Berndt, T., Sipila, M., Paasonen, P., Petaja, T., Kim, S., Kurten, T., Stratmann, F.,
569 Kerminen, V., and Kulmala, M.: A new atmospherically relevant oxidant of sulphur dioxide,
570 *Nature*, 488, 193-196, <https://doi.org/10.1038/nature11278>, 2012.
- 571 Mukuta, T., Fukazawa, N., Murata, K., Inagaki, A., Akita, M., Tanaka, S., Koshihara, S. Y., and
572 Onda, K.: Infrared vibrational spectroscopy of [Ru(bpy)₂(bpm)]²⁺ and [Ru(bpy)₃]²⁺ in the
573 excited triplet state, *Inorg. Chem.*, 53, 2481-2490, <https://doi.org/10.1021/ic402474t>, 2014.
- 574 Olson, E., Michalski, G., Welp, L., Valdivia, A., Larico, J., Pen, J., Fang, H., Gomez, K., and
575 Li, J.: Mineral dust and fossil fuel combustion dominate sources of aerosol sulfate in urban
576 Peru identified by sulfur stable isotopes and water-soluble ions, *Atmos. Environ.*, 260,
577 118482-118495, <https://doi.org/10.1016/j.atmosenv.2021.118482>, 2021.
- 578 Park, J. and Jang, M.: Heterogeneous photooxidation of sulfur dioxide in the presence of
579 airborne mineral dust particles, *RSC Adv.*, 6, 58617-58627,
580 <https://doi.org/10.1039/c6ra09601h>, 2016.
- 581 Park, J., Jang, M., and Yu, Z.: Heterogeneous photo-oxidation of SO₂ in the presence of two



- 582 different mineral dust particles: Gobi and arizona dust, *Environ. Sci. Technol.*, 51, 9605-
583 9613, <https://doi.org/10.1021/acs.est.7b00588>, 2017.
- 584 Peng, Y., von Salzen, K., and Li, J.: Simulation of mineral dust aerosol with Piecewise Log-
585 normal Approximation (PLA) in CanAM4-PAM, *Atmos. Chem. Phys.*, 12, 6891-6914,
586 <https://doi.org/10.5194/acp-12-6891-2012>, 2012.
- 587 Prospero, J.: Long-range transport of mineral dust in the global atmosphere: Impact of African
588 dust on the environment of the southeastern United States, *Proc. Natl. Acad. Sci. U. S. A.*,
589 96, 3396-3403, <https://doi.org/10.1073/pnas.96.7.3396>, 1999.
- 590 Shao, J., Chen, Q., Wang, Y., Lu, X., He, P., Sun, Y., Shah, V., Martin, R. V., Philip, S., Song,
591 S., Zhao, Y., Xie, Z., Zhang, L., and Alexander, B.: Heterogeneous sulfate aerosol formation
592 mechanisms during wintertime Chinese haze events: air quality model assessment using
593 observations of sulfate oxygen isotopes in Beijing, *Atmos. Chem. Phys.*, 19, 6107-6123,
594 <https://doi.org/10.5194/acp-19-6107-2019>, 2019.
- 595 Shiraiwa, M., Ueda, K., Pozzer, A., Lammel, G., Kampf, C. J., Fushimi, A., Enami, S., Arangio,
596 A. M., Frohlich-Nowoisky, J., Fujitani, Y., Furuyama, A., Lakey, P. S. J., Lelieveld, J., Lucas,
597 K., Morino, Y., Poschl, U., Takahama, S., Takami, A., Tong, H., Weber, B., Yoshino, A., and
598 Sato, K.: Aerosol health effects from molecular to global scales, *Environ. Sci. Technol.*, 51,
599 13545-13567, <https://doi.org/10.1021/acs.est.7b04417>, 2017.
- 600 Sidebottom, H. W., Badcock, C. C., Jackson, G. E., Calvert, J. G., Reinhardt, G. W., and Damon,
601 E. K.: Photooxidation of sulfur dioxide, *Environ. Sci. Technol.*, 6, 72-79,
602 <https://doi.org/10.1080/00022470.1971.10469552>, 1972.
- 603 Solbrig, C. W. and Gidaspow, D.: Convective diffusion in a parallel plate duct with one catalytic
604 wall, laminar flow, first order reaction-part one, *Can. J. Chem. Eng.*, 45, 35-39,
605 [https://doi.org/10.1016/0304-5102\(89\)80197-X](https://doi.org/10.1016/0304-5102(89)80197-X), 1967.
- 606 Sumner, A. L., Menke, E. J., Dubowski, Y., Newberg, J. T., Penner, R. M., Hemminger, J. C.,
607 Wingen, L. M., Brauers, T. and Finlayson-Pitts, B. J. The nature of water on surfaces of
608 laboratory systems and implications for heterogeneous chemistry in the troposphere. *Phys.*
609 *Chem. Chem. Phys.*, 6, 604-613, <https://doi.org/10.1039/B308125G>, 2004.
- 610 Tohidi, R., Farahani, V., and Sioutas, C.: Real-time measurements of mineral dust concentration
611 in coarse particulate matter PM_{10-2.5} by employing a novel optical-based technique in Los
612 Angeles, *Sci. Total. Environ.*, 838, 156215-156226, <https://doi.org/10.1016/j.scitotenv.2022.156215>, 2022.
- 614 Urupina, D., Romanias, M. N., and Thevenet, F.: How relevant is it to use mineral proxies to
615 mimic the atmospheric reactivity of natural dust samples? A reactivity study using SO₂ as
616 probe molecule, *Minerals*, 11, 282-299, <https://doi.org/10.3390/min11030282>, 2021.
- 617 Urupina, D., Lasne, J., Romanias, M. N., Thiery, V., Dagsson-Waldhauserova, P., and Thevenet,
618 F.: Uptake and surface chemistry of SO₂ on natural volcanic dusts, *Atmos. Environ.*, 217,
619 116942-116959, <https://doi.org/10.1016/j.atmosenv.2019.116942>, 2019.
- 620 Usher, C., Michel, A., and Grassian, V.: Reactions on mineral dust, *Chem. Rev.*, 103, 4883-
621 4939, <https://doi.org/10.1021/cr020657y>, 2003.
- 622 Usher, C., Al-Hosney, H., Carlos-Cuellar, S., and Grassian, V.: A laboratory study of the
623 heterogeneous uptake and oxidation of sulfur dioxide on mineral dust particles, *J. Geophys.*



- 624 Res-atmos. , 107, 4713-4729, <https://doi.org/10.1029/2002jd002051>, 2002.
- 625 Wang, J., Li, J., Ye, J., Zhao, J., Wu, Y., Hu, J., Liu, D., Nie, D., Shen, F., Huang, X., Huang,
626 D. D., Ji, D., Sun, X., Xu, W., Guo, J., Song, S., Qin, Y., Liu, P., Turner, J. R., Lee, H. C.,
627 Hwang, S., Liao, H., Martin, S. T., Zhang, Q., Chen, M., Sun, Y., Ge, X., and Jacob, D. J.:
628 Fast sulfate formation from oxidation of SO₂ by NO₂ and HONO observed in Beijing haze,
629 Nat. Commun., 11, 2844-2850, <https://doi.org/10.1038/s41467-020-16683-x>, 2020a.
- 630 Wang, T., Liu, Y., Deng, Y., Fu, H., Zhang, L., and Chen, J.: The influence of temperature on
631 the heterogeneous uptake of SO₂ on hematite particles, Sci. Total. Environ., 644, 1493-1502,
632 <https://doi.org/10.1016/j.scitotenv.2018.07.046>, 2018.
- 633 Wang, T., Liu, Y. Y., Deng, Y., Cheng, H. Y., Yang, Y., Li, K. J., Fang, X. Z., and Zhang, L. W.:
634 Irradiation intensity dependent heterogeneous formation of sulfate and dissolution of ZnO
635 nanoparticles, Environ. Sci.: Nano, 7, 327-338, <https://doi.org/10.1039/c9en01148j>, 2020b.
- 636 Wang, Z., Wang, T., Fu, H., Zhang, L., Tang, M., George, C., Grassian, V. H., and Chen, J.:
637 Enhanced heterogeneous uptake of sulfur dioxide on mineral particles through modification
638 of iron speciation during simulated cloud processing, Atmos. Chem. Phys., 19, 12569-12585,
639 <https://doi.org/10.5194/acp-19-12569-2019>, 2019.
- 640 Xue, J., Yuan, Z., Griffith, S. M., Yu, X., Lau, A. K., and Yu, J. Z.: Sulfate formation enhanced
641 by a cocktail of high NO_x, SO₂, particulate matter, and droplet pH during haze-fog events
642 in megacities in china: An observation-based modeling investigation, Environ. Sci. Technol.,
643 50, 7325-7334, <https://doi.org/10.1021/acs.est.6b00768>, 2016.
- 644 Yang, N., Tsona, N. T., Cheng, S., Li, S., Xu, L., Wang, Y., Wu, L., and Du, L.: Competitive
645 reactions of SO₂ and acetic acid on α -Al₂O₃ and CaCO₃ particles, Sci. Total. Environ., 699,
646 134362-134370, <https://doi.org/10.1016/j.scitotenv.2019.134362>, 2020.
- 647 Yang, W., Ma, Q., Liu, Y., Ma, J., Chu, B., and He, H.: The effect of water on the heterogeneous
648 reactions of SO₂ and NH₃ on the surfaces of α -Fe₂O₃ and γ -Al₂O₃, Environ. Sci.: Nano, 6,
649 2749-2758, <https://doi.org/10.1039/c9en00574a>, 2019.
- 650 Ye, C., Chen, H., Hoffmann, E. H., Mettke, P., Tilgner, A., He, L., Mutzel, A., Bruggemann,
651 M., Poulain, L., Schaefer, T., Heinold, B., Ma, Z., Liu, P., Xue, C., Zhao, X., Zhang, C.,
652 Zhang, F., Sun, H., Li, Q., Wang, L., Yang, X., Wang, J., Liu, C., Xing, C., Mu, Y., Chen, J.,
653 and Herrmann, H.: Particle-phase photoreactions of HULIS and TMIs establish a strong
654 source of H₂O₂ and particulate sulfate in the winter north china plain, Environ. Sci. Technol.,
655 55, 7818-7830, <https://doi.org/10.1021/acs.est.1c00561>, 2021.
- 656 Zhang, P., Chen, T., Ma, Q., Chu, B., Wang, Y., Mu, Y., Yu, Y., and He, H.: Diesel soot
657 photooxidation enhances the heterogeneous formation of H₂SO₄, Nat. Commun., 13, 5364-
658 5372, <https://doi.org/10.1038/s41467-022-33120-3>, 2022.
- 659 Zhang, R., Gen, M., Huang, D., Li, Y., and Chan, C.: Enhanced sulfate production by nitrate
660 photolysis in the presence of halide ions in atmospheric particles, Environ. Sci. Technol.,
661 54, 3831-3839, <https://doi.org/10.1021/acs.est.9b06445>, 2020a.
- 662 Zhang, T., Yang, W., Han, C., Yang, H., and Xue, X.: Heterogeneous reaction of ozone with
663 syringic acid: Uptake of O₃ and changes in the composition and optical property of syringic
664 acid, Environ. Pollut., 257, 113632-113638, <https://doi.org/10.1016/j.envpol.2019.113632>,
665 2020b.



- 666 Zhang, X., Zhuang, G., Chen, J., Wang, Y., Wang, X., An, Z., and Zhang, P.: Heterogeneous
667 reactions of sulfur dioxide on typical mineral particles, *J. Phys. Chem. B*, 110, 12588-12596,
668 <https://doi.org/>, 2006.
- 669 Zhang, Y., Bao, F., Li, M., Chen, C., and Zhao, J.: Nitrate-enhanced oxidation of SO₂ on mineral
670 dust: A vital role of a proton, *Environ. Sci. Technol.*, 53, 10139-10145,
671 <https://doi.org/10.1021/acs.est.9b01921>, 2019.
- 672 Zhang, Y., Bao, F., Li, M., Xia, H., Huang, D., Chen, C., and Zhao, J.: Photoinduced uptake
673 and oxidation of SO₂ on Beijing urban PM_{2.5}, *Environ. Sci. Technol.*, 54, 14868-14876,
674 <https://doi.org/10.1021/acs.est.0c01532>, 2020c.
- 675